



**HAL**  
open science

## Automatic quality control of brain T1-weighted magnetic resonance images for a clinical data warehouse

Simona Bottani, Ninon Burgos, Aurélien Maire, Adam Wild, Sébastien Ströer, Didier Dormont, Olivier Colliot

### ► To cite this version:

Simona Bottani, Ninon Burgos, Aurélien Maire, Adam Wild, Sébastien Ströer, et al.. Automatic quality control of brain T1-weighted magnetic resonance images for a clinical data warehouse. *Medical Image Analysis*, 2022, 75, 10.1016/j.media.2021.102219 . hal-03154792v4

**HAL Id: hal-03154792**

**<https://inria.hal.science/hal-03154792v4>**

Submitted on 29 Aug 2021

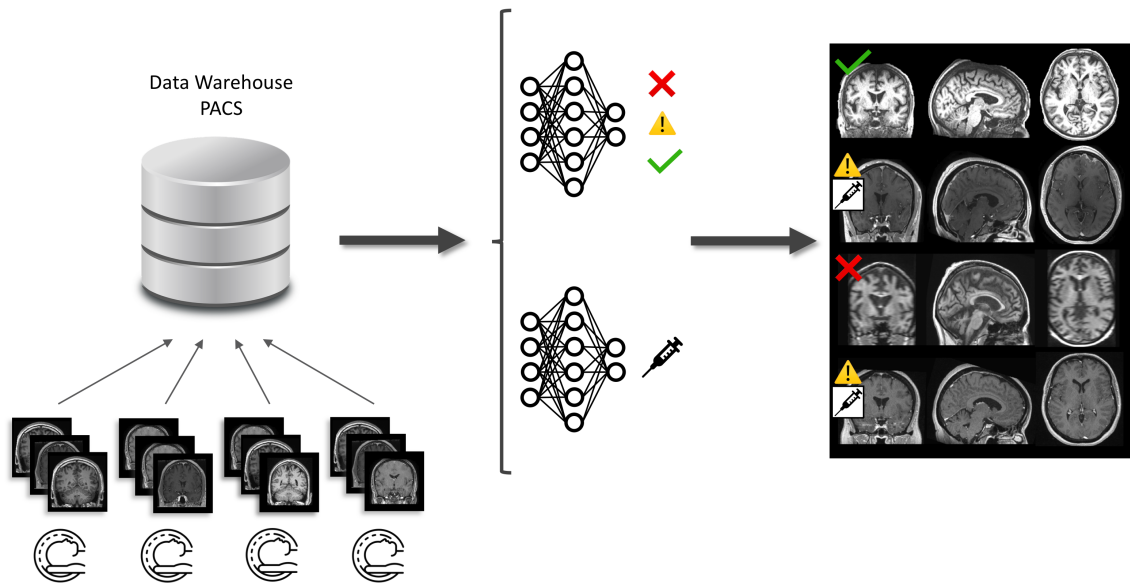
**HAL** is a multi-disciplinary open access archive for the deposit and dissemination of scientific research documents, whether they are published or not. The documents may come from teaching and research institutions in France or abroad, or from public or private research centers.

L'archive ouverte pluridisciplinaire **HAL**, est destinée au dépôt et à la diffusion de documents scientifiques de niveau recherche, publiés ou non, émanant des établissements d'enseignement et de recherche français ou étrangers, des laboratoires publics ou privés.

# Graphical Abstract

## Automatic quality control of brain T1-weighted magnetic resonance images for a clinical data warehouse

Simona Bottani, Ninon Burgos, Aurélien Maire, Adam Wild, Sebastian Ströer, Didier Dormont, Olivier Colliot, APPRIMAGE Study Group



## Highlights

### **Automatic quality control of brain T1-weighted magnetic resonance images for a clinical data warehouse**

Simona Bottani, Ninon Burgos, Aurélien Maire, Adam Wild, Sebastian Ströer, Didier Dormont, Olivier Colliot, APPRIMAGE Study Group

- We propose a framework for the automatic QC of 3D T1w brain MRI for a clinical data warehouse.
- We manually labeled 5500 images to train/test different convolutional neural networks.
- The automatic approach can identify images which are not proper T1w brain MRIs (e.g. truncated images).
- It is able to identify acquisitions for which gadolinium was injected.
- It can also accurately identify low quality images.

# Automatic quality control of brain T1-weighted magnetic resonance images for a clinical data warehouse

Simona Bottani<sup>a,b,c,d,e,f</sup>, Ninon Burgos<sup>b,c,d,e,f,a</sup>, Aurélien Maire<sup>g</sup>, Adam Wild<sup>b,c,d,e,f,a</sup>, Sebastian Ströer<sup>h</sup>, Didier Dormont<sup>b,c,d,e,f,a,h</sup>, Olivier Colliot<sup>b,c,d,e,f,a</sup>, APPRIMAGE Study Group

<sup>a</sup>*Inria, Aramis project-team, Paris, 75013, France*

<sup>b</sup>*Sorbonne Université, Paris, 75013, France*

<sup>c</sup>*Institut du Cerveau - Paris Brain Institute - ICM, Paris, 75013, France*

<sup>d</sup>*Inserm, Paris, 75013, France*

<sup>e</sup>*CNRS, Paris, 75013, France*

<sup>f</sup>*AP-HP, Hôpital de la Pitié Salpêtrière, Paris, 75013, France*

<sup>g</sup>*AP-HP, WIND department, Paris, 75012, France*

<sup>h</sup>*AP-HP, Hôpital de la Pitié Salpêtrière, Department of Neuroradiology, Paris, 75013, France*

---

## Abstract

Many studies on machine learning (ML) for computer-aided diagnosis have so far been mostly restricted to high-quality research data. Clinical data warehouses, gathering routine examinations from hospitals, offer great promises for training and validation of ML models in a realistic setting. However, the use of such clinical data warehouses requires quality control (QC) tools. Visual QC by experts is time-consuming and does not scale to large datasets. In this paper, we propose a convolutional neural network (CNN) for the automatic QC of 3D T1-weighted brain MRI for a large heterogeneous clinical data warehouse. To that purpose, we used the data warehouse of the hospitals of the Greater Paris area (Assistance Publique-Hôpitaux de Paris [AP-HP]). Specifically, the objectives were: 1) to identify images which are not proper

T1-weighted brain MRIs; 2) to identify acquisitions for which gadolinium was injected; 3) to rate the overall image quality. We used 5000 images for training and validation and a separate set of 500 images for testing. In order to train/validate the CNN, the data were annotated by two trained raters according to a visual QC protocol that we specifically designed for application in the setting of a data warehouse. For objectives 1 and 2, our approach achieved excellent accuracy (balanced accuracy and F1-score  $>90\%$ ), similar to the human raters. For objective 3, the performance was good but substantially lower than that of human raters. Nevertheless, the automatic approach accurately identified (balanced accuracy and F1-score  $>80\%$ ) low quality images, which would typically need to be excluded. Overall, our approach shall be useful for exploiting hospital data warehouses in medical image computing.

*Keywords:* Quality control, Clinical data warehouse, Brain MRI, Deep learning

---

## 1. Introduction

Structural T1-weighted (T1w) magnetic resonance imaging (MRI) is useful for diagnosis of various brain disorders, in particular neurodegenerative diseases (Frisoni et al., 2010; Harper et al., 2016). They have thus often been used as inputs of machine learning (ML) algorithms for computer-aided diagnosis (CAD) (Falahati et al., 2014; Koikkalainen et al., 2016; Rathore et al., 2017; Burgos and Colliot, 2020).

Most ML methods are trained and validated on high-quality research data (Noor et al., 2019; Choi et al., 2019; Punjabi et al., 2019): protocols for image acquisition are standardized and a strict quality control is applied (Jack et al., 2008; Littlejohns et al., 2020). However, to be applied in the clinic, ML methods need to be validated on clinical routine images. In recent years, hospitals have constituted clinical data warehouses that can contain medical images from 100,000-1,000,000 patients (Daniel and Salamanca, 2020; Amara et al., 2020). The quality of such images can greatly vary (see Figure 2), since the acquisition protocols are not standardized, scanners may not be recent and patients may have moved during the acquisition. All these factors can prevent algorithms from working properly (Reuter et al., 2015; Gilmore et al., 2019). Quality control (QC) is thus a fundamental step before training and evaluating ML approaches on clinical routine data.

Manual QC takes time and is thus not always doable, especially in the context of ML-based CAD, where a large number of training samples is needed. Typically, clinical data warehouses can contain hundreds of thousands of samples. Even if web-based systems facilitate annotation (Kim et al., 2019; Keshavan et al., 2018), the task remains unfeasible for very large datasets. In this context, automatic QC is needed.

Several works have been proposed to enable automatic QC of cerebral MR images. The Preprocessed Connectomes Project developed a Quality

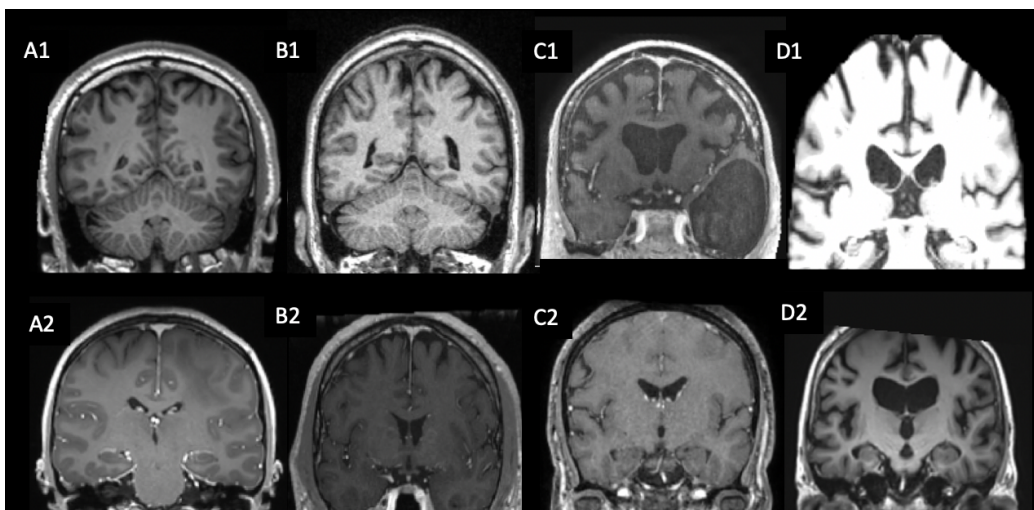


Figure 1: Examples of T1w brain images from the clinical data warehouse and the corresponding labels. A1: Image of good quality (tier 1), without gadolinium; A2: Good quality (tier 1), with gadolinium; B1: Medium quality (tier 2), without gadolinium (noise grade 1); B2: Medium quality (tier 2), with gadolinium (contrast grade 1); C1: Bad quality (tier 3), without gadolinium (contrast grade 2, motion grade 2); C2: Bad quality (tier 3), with gadolinium (contrast grade 2, motion grade 1); D1: Straight rejection (segmented); D2: Straight rejection (cropped).

Assessment Protocol<sup>1</sup>. The package enables the extraction of several image quality metrics (IQMs) such as the signal-to-noise ratio, the contrast-to-noise ratio or the volume of the gray and white matter. IQMs are then compared to a normative distribution obtained from three research datasets, ABIDE (Di Martino et al., 2014), CoRR<sup>2</sup> and NFB<sup>3</sup>. In the same spirit, we find (Esteban et al., 2017; Alfaro-Almagro et al., 2018; Raamana et al., 2020). These approaches propose to use the IQMs as input of a classifier for automatic QC.

<sup>1</sup><http://preprocessed-connectomes-project.org/quality-assessment-protocol>

<sup>2</sup>[http://fcon\\_1000.projects.nitrc.org/indi/CoRR/html/index.html](http://fcon_1000.projects.nitrc.org/indi/CoRR/html/index.html)

<sup>3</sup>[http://fcon\\_1000.projects.nitrc.org/indi/enhanced/](http://fcon_1000.projects.nitrc.org/indi/enhanced/)

Esteban et al. (2017) and Alfaro-Almagro et al. (2018) developed a pipeline for the automatic QC of 3D brain T1w MRI, the first has the advantage to be an open source software (called MRIQC). Raamana et al. (2020) developed another open source software called VisualQC whose aim is the visualisation and the rating of the Freesurfer cortical segmentation output. The pipelines proposed by these works are very extensive as they require registration and segmentation steps to extract features. It is not possible to assume a priori that these steps will perform well with a new unseen clinical dataset. On the contrary, it is likely that the segmentation will fail for the lowest quality images, thus making it impossible to apply the QC tool. Moreover, the extracted features may not be representative of the problems affecting clinical routine data. As proposed by Sujit et al. (2019), convolutional neural networks (CNNs) are a good option for automatic QC because they can learn features without knowing a priori which are the most adapted. A further limitation of these works is that they rely on images acquired following a well-defined research protocol. The pipeline presented in (Alfaro-Almagro et al., 2018) was developed for the large, but well-standardized, UK Biobank dataset containing mostly healthy volunteers. Esteban et al. (2017) and Sujit et al. (2019) trained their algorithms on ABIDE, a research multicenter study including patients with autism and control subjects and used another research dataset for testing. These datasets are both smaller and less realistic than a clinical dataset. In particular, Sujit et al. (2019) used 2D slices as input for the model and they classified their images only in two classes:

acceptable or not acceptable.

More studies can be found if we enlarge the scope to other body parts or imaging sequences. Deep learning models have been developed for different modalities, different organs and different QC tasks: for the QC of mammograms (Kretz et al., 2020), fetal ultrasound cardiac images (Dong et al., 2019), and brain diffusion MRI (Graham et al., 2018), for the detection of artefacts on cardiac MRI (Oksuz et al., 2019) and blurring on histological images (Campanella et al., 2018). Several works used a classifier trained on image quality metrics (IQM) extracted from the images: Küstner et al. (2018); Sadri et al. (2020) used this approach with a research dataset composed of different body parts and MRI sequences, Tayari et al. (2019) applied it to 3D 1H MR spectroscopy of the prostate and Janowczyk et al. (2019) developed a tool called HistoQC for the QC of histological images. Finally, some works focused on the QC of post-processing results, mainly segmentation results. It can be done extracting IQMs from the segmented images, as proposed by Alba et al. (2018) for cardiac images, or using deep learning models as done by Robinson et al. (2018, 2019) for cardiac images from the UK Biobank dataset, which contains more than 10,000 samples, and Sunoqrot et al. (2020) for prostate images.

To the best of our knowledge, there is currently no automatic QC approach dedicated to large clinical datasets of brain MRI. Our work was done using a clinical data warehouse that assembles all MRI data from all hospitals of the greater Paris area. Images come from different sites and different ma-

chines with no homogenization on the parameters, and their acquisition cover several decades. The patient may have any disease for which a brain MRI exam is required. All these factors are not present in the approaches already proposed in the literature: even when images come from different sites, the acquisition protocol is harmonized, the number of machines is limited and they are usually acquired within a few years, avoiding intrinsic problems of quality due to the progress in the technology. Additionally, the presence of different diseases such as neurodegenerative diseases, stroke, multiple sclerosis, or brain tumours, is typical of clinical datasets: they can strongly alter the structure of the brain and it may be difficult to use a specific set of features to characterize the quality of the images independently of the disease. In addition, due to security reasons, images from the data warehouse cannot be uploaded to a web server and we had to work in a restricted IT environment (Daniel and Salamanca, 2020).

The objective of our work was to develop a method for the automatic QC of T1w brain MRI in large clinical data warehouses. The specific objectives were to: 1) discard images which are not proper T1w brain MRI; 2) identify images with gadolinium; 3) recognise images of bad, medium and good quality. We used 5000 images for training/validation and 500 for testing. To train/validate the models, the data were annotated by two trained raters. To that purpose, we introduced an original visual QC protocol that is applicable to clinical data warehouses. Figure 2 presents an overview of our work.

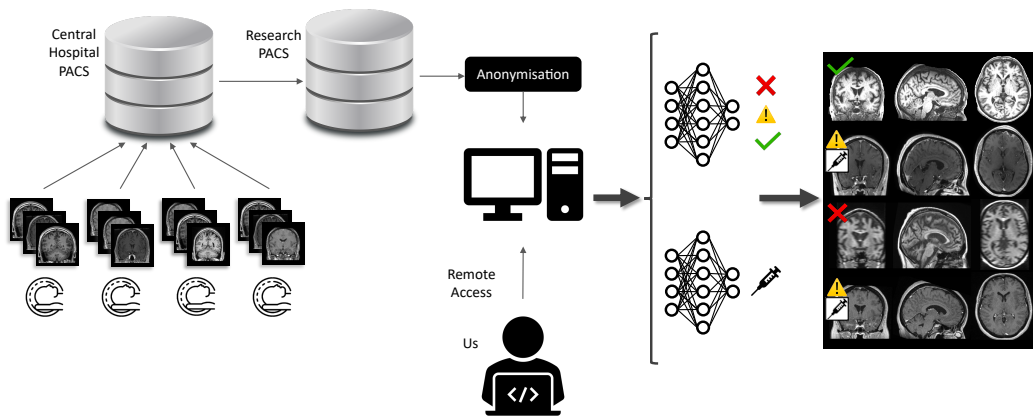


Figure 2: General workflow of the proposed QC framework. Images were acquired as part of the routine clinical care in different hospital sites and gathered in a central hospital PACS. Images relevant to our research project were copied to the research PACS and anonymized. They always remain within the hospital network that we accessed remotely. Thanks to the connection to the hospital IT network, we manually labeled the images before training and testing our deep learning models.

## 2. Materials and methods

### 2.1. Dataset description

This work relies on a large clinical routine dataset containing all the T1w brain MR images of adult patients scanned in hospitals of the Greater Paris area (Assistance Publique-Hôpitaux de Paris [AP-HP]). The data were made available by the data warehouse of the AP-HP and the study was approved by the Ethical and Scientific Board of the AP-HP. According to French regulation, consent was waived as these images were acquired as part of the routine clinical care of the patients.

All the images were already stored in a single central clinical PACS. Then, the data warehouse team of the AP-HP made a query on the central clinical

PACS and copied the images to the so-called “research PACS”. Note that, in spite of its name, the research PACS is also within the hospital network. The images were then pseudonymized: the DICOM fields that contained information about the patient or the physician who performed the exam, such as their name or identifier were erased. For further anonymization, the date of the exam and the date of birth were also erased from the DICOM fields. Nevertheless, as mentioned below, this information was available from another database (but not for all patients). In this other database, to increase anonymization, the date of the exam and the date of birth were also changed (they were shifted by a constant in order to keep the age information accurate). Note that data were accessed remotely and that all the analyses (including training and inference of deep learning models on GPUs) were performed within the hospital network, as exporting data outside of this network is not allowed. This is summarized in Figure 2.

The images were selected according to DICOM attributes. A first query on the PACS was performed to list the DICOM attributes corresponding to MRI. For all the MR images, we listed the “series descriptions”, “body parts examined”, and “study descriptions” DICOM attributes. A neuroradiologist manually selected all the attribute values that may refer to 3D T1w brain MRI (e.g. “T1 EG 3D MPR”, “SAG 3D BRAVO”, “3D T1 EG MPAGE”, “IRM cranio”, “Brain T1W/FFEGADO”). He selected 3736 relevant attribute values. In case of a doubt, the neuroradiologist kept the value to avoid discarding potential images of interest. Relevant attribute values were

manually selected since some of the information present in the DICOM fields is filled manually by the radiology department or even by the radiographer who is performing the exam. Standardization exists within a given hospital but our data came from 39 different hospitals, which all have different conventions. Even within a hospital, there was still a large variability, probably because different MRI protocols for a head/brain examination exist and there was no specific effort to name the body part in a consistent way across them. It could also be that these had spelling errors or that they were not changed during an exam (resulting in the annotation of gadolinium injection even when it is not present or the opposite).

Among all the 3D T1w brain MRI of the AP-HP, a first batch of about 11,000 images was delivered by the data warehouse. We excluded all the images having less than 40 slices because they correspond to 2D brain images even if the corresponding DICOM attribute refer to 3D. For the present study, we randomly selected 5500 images, corresponding to 4177 patients. The images were acquired on various scanners from four manufacturers: Siemens Healthineers ( $n = 3752$ ), GE Healthcare ( $n = 1710$ ), Philips ( $n = 33$ ) and Toshiba ( $n = 5$ ). Among all the images, 3229 images were acquired with 3 Tesla machines and 2271 with 1.5 Tesla. From the 5500 images, age and gender information was known only for 4274 images, corresponding to 3169 patients. This is explained by the fact that, while images are stored on the PACS, socio-demographic and clinical data are stored using another software system that had been installed later in the different hospitals. Furthermore,

age and sex in the DICOM header were erased during the pseudonymization process. Among the 4274 images, we have 2297 women, 1968 men and 9 patients with unknown sex, with an average age of  $55.15 \pm 7.89$  (min: 18, max: 95). Table 1 reports all the scanner models present in our dataset with the corresponding magnetic field strength for the 5500 images and the corresponding age range and sex for the images for which this information is available.

## 2.2. Image preprocessing

The T1w MR images were converted from DICOM to NIfTI using the software `dicom2niix` (Li et al., 2016) and organized using the Brain Imaging Data Structure (BIDS) standard (Gorgolewski et al., 2016). Images with a voxel dimension smaller than 0.9 mm were resampled using a 3rd-order spline interpolation to obtain 1 mm isotropic voxels. To facilitate annotations, we applied the following pre-processing using the ‘t1-linear’ pipeline of Clinica (Routier et al., 2021), which is a wrapper of the ANTs software (Avants et al., 2014). Bias field correction was applied using the N4ITK method (Tustison et al., 2010). An affine registration to MNI space was performed using the SyN algorithm (Avants et al., 2008). The registered images were further rescaled based on the min and max intensity values ( $y = (x - \min(x))/(\max(x) - \min(x))$ , where  $x$  is the T1w brain MRI in the MNI space). Images were then cropped to remove background resulting in images of size  $169 \times 208 \times 179$ , with 1 mm isotropic voxels (Wen et al.,

Table 1: Model name of all the scanners, grouped by manufacturer, with the corresponding magnetic field strength (T) and the number of images. Age (mean  $\pm$  std[range]) and sex (number of females [F] / males [M]) are reported when available for each model. As indicated in the text, from the 5500 images, age and gender information were available only for 4274 images. Thus, this information was left blank when it was available for none of the images of a given scanner model.

	Model Name	T	N images	Age (mean $\pm$ std [range])	Sex (F/M)
Siemens	Aera	1.5	489	53.53 $\pm$ 18.00 [18, 95]	223 / 142
	Amira	1.5	29	47.81 $\pm$ 13.57 [19, 68]	6 / 10
	Avanto	1.5	603	52.79 $\pm$ 15.39 [18, 88]	164 / 125
	Avanto.fit	1.5	81	56.06 $\pm$ 16.64 [19, 88]	34 / 28
	Biograph mMR	3	12	-	-
	Espree	1.5	1	-	-
	Magnetom Vida	3	3	-	-
	Magnetom Essenza	1.5	11	37.2 $\pm$ 15.93 [22, 69]	1 / 9
	Sempre	1.5	3	45 $\pm$ 0 [45]	1 / 0
	Skyra	3	1851	54.31 $\pm$ 17.56 [18, 95]	708 / 692
	Spectra	3	23	55.13 $\pm$ 18.87 [22, 66]	2 / 6
	Symphony	1.5	3	-	-
Verio	3	643	55.65 $\pm$ 17.75 [18, 92]	310 / 294	
GE Healthcare	Discovery MR450	1.5	4	40.67 $\pm$ 23.57 [24, 74]	1 / 2
	Discovery MR750(w)	3	675	55.52 $\pm$ 17.49 [18, 93]	240 / 256
	Optima MR360	1.5	2	63 $\pm$ 0 [63]	0 / 1
	Optima MR450w	1.5	284	59.80 $\pm$ 18.0 [18, 95]	160 / 97
	Signa Architect	1.5	243	52.14 $\pm$ 18.63 [19, 92]	128 / 99
	Signa Artist	1.5	4	88.0 $\pm$ 1.41 [86, 89]	2 / 2
	Signa Excite	1.5	3	30.5 $\pm$ 4.5 [26, 35]	2 / 0
	Signa Explorer	1.5	1	76 $\pm$ 0 [76]	1 / 0
	Signa HDx(t)	1.5	489	61.53 $\pm$ 18.34 [18, 94]	250 / 166
	Signa Pioneer	3	1	76 $\pm$ 0 [76]	0 / 1
	Signa Voyager	1.5	1	-	-
	Unknown	1.5	3	-	-
Philips	Achieva	3	21	51.0 $\pm$ 14.0 [27, 70]	5 / 2
	Ingenia	1.5	5	81.13 $\pm$ 12.20 [64, 92]	1 / 2
	Intera	1.5	7	61 $\pm$ 0 [61]	2 / 0
Toshiba	Titan	1.5	2	54.5 $\pm$ 1.5 [53, 56]	2 / 0
	Vantage Elan	1.5	3 12	55.5 $\pm$ 3.5 [52, 59]	1 / 1

2020). One should note that we only aimed to obtain a rough alignment and intensity rescaling to facilitate annotation.

### *2.3. Manual labeling of the dataset*

In this section, we introduce the visual QC protocol. We describe the different characteristics noted on the images and how we created the final label for the automatic QC. Images were labeled by two trained raters and the annotation protocol was designed with the help of a radiologist.

#### *2.3.1. Quality criteria*

Five characteristics were manually annotated. The first two (straight rejection and gadolinium) are binary flags, while the other three (motion, contrast and noise) are assessed with a three-level grade.

- **Straight rejection (SR):** images not containing a T1w MRI of the whole brain (for instance images of segmented tissues or truncated images). Note that these images still have DICOM attributes corresponding to T1w brain MRI and thus were not removed through the selection step based on DICOM attributes.
- **Gadolinium:** presence of gadolinium-based contrast agent.
- **Motion** 0: no motion, 1: some motion but the structures of the brain are still distinguishable, 2: severe motion, the cortical and subcortical structures are difficult to distinguish.

- **Contrast** 0: good contrast, 1: medium contrast (gray matter and white matter are difficult to distinguish in some parts of the image), 2: bad contrast (gray matter and white matter are difficult to distinguish everywhere in the brain).
- **Noise** 0: no noise, 1: presence of noise that does not prevent identifying structures, 2: severe noise that does prevent identifying structures.

Gadolinium injection, motion, contrast and noise were noted for all the images which were not defined as SR. According to the grades given to the motion, contrast and noise characteristics, we determined three tiers corresponding to images of good, medium and bad quality. The tiers, along with the rules used to defined them, are described in Table 2.

<b>Tier</b>	<b>Description</b>	<b>Determination rule</b>
Tier 1	3D T1w brain MRI of good quality	Grade 0 for motion, contrast and noise
Tier 2	3D T1w brain MRI of medium quality	At least one characteristic among motion, contrast and noise with grade 1 and none with grade 2
Tier 3	3D T1w brain MRI of bad quality	At least one characteristic among motion, contrast and noise with grade 2

Table 2: Description and determination rules of the proposed quality control tiers.

### *2.3.2. Annotation set-up*

Our aim was to annotate the largest possible number of images in an efficient manner while being restricted to the environment of the data warehouse which only included a Jupyter notebook and a command-line interface. We thus implemented a graphical interface in a Jupyter notebook. This interface displayed only the central axial, sagittal and coronal slices of the brain. Indeed, loading the whole 3D volume for inspecting all the slices in the data warehouse environment was unfeasible due to the above mentioned restrictions. Specifically, from the NIfTI format, we saved a screenshot of the central slice of each view (sagittal, coronal, axial) in PNG format. This allowed a fast loading of the image to annotate. Each image was labeled by two trained raters. The interface was flexible: it was possible to go back and label again an image, and after the labelling all the characteristics noted were displayed. The procedure was optimized to reduce the workload of the raters to a minimum. The implementation is available on a GitHub repository: [https://github.com/SimonaBottani/Quality\\_Control\\_Interface](https://github.com/SimonaBottani/Quality_Control_Interface).

### *2.3.3. Consensus label*

The final label used to train and validate the automatic QC is a consensus between the two raters. If the users labeled different image characteristics, we determined a procedure to define a consensus label. We distinguished two types of disagreement: one regarding the SR status and the other one regarding the other characteristics based on which the tiers are assigned. When the

two raters disagreed on the SR status, we manually set the consensus label: the two raters reviewed the images and decided together to keep the SR label or assign the alternative label. In case of disagreement regarding the other characteristics, the consensus was chosen as follows. The objective was to be as conservative as possible: we wanted to retain all the imperfections that may have been seen by one annotator and not by the other. For a given characteristic, the consensus grade was chosen as the maximum of the two grades of the observers. The tier was recomputed accordingly.

#### *2.4. Automatic quality control method*

We developed an automatic QC method based on CNNs trained to perform several classification tasks: 1) discard images which were not proper T1w brain MRI (SR: yes vs no); 2) identify images with gadolinium (gadolinium: yes vs no); 3) differentiate images of bad quality from images of medium and good quality (tier 3 vs tiers 2-1); 4) differentiate images of medium quality from images of good quality (tier 2 vs tier 1).

##### *2.4.1. Network architecture*

The network proposed was composed of five convolutional blocks and of three fully connected layers. The convolutional blocks were made of one convolutional layer, one batch normalization layer, one ReLU and one max pooling. Details about architecture are represented on Figure 3. All the details about the parameters of the layers, i.e. the filter size, the number of filters/neurons, the stride and the padding size and the dropout rate are

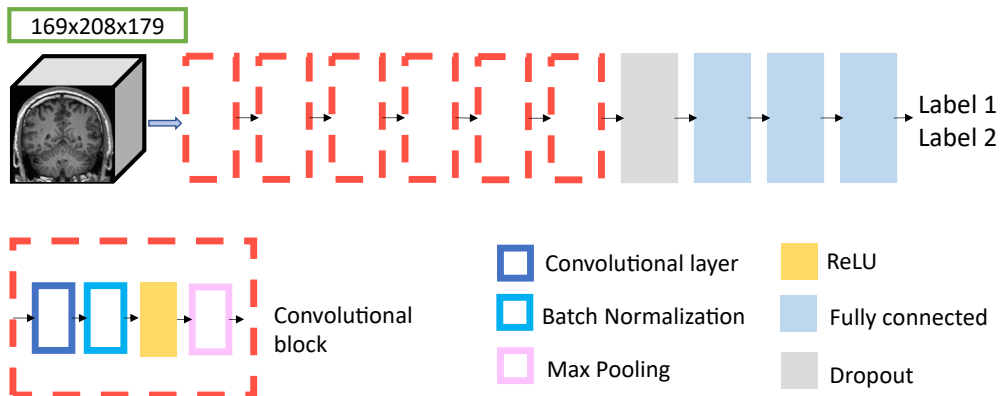


Figure 3: Architecture of the 3D CNN called Conv5\_FC3. Five convolutional blocks (composed sequentially of a convolutional layer, a batch normalization layer, a ReLU and a max pooling layer) are followed by a dropout and three fully connected layers.

in the Supplementary Materials in table S2. In the following, we refer to this architecture as Conv5\_FC3. The models were trained using the cross entropy loss, which was weighted according to the proportion of images per class for each task. We used the Adam optimizer with a learning rate of  $1e-4$ . We implemented early stopping and all the models were evaluated with a maximum of 50 epochs. The batch size was set to 2. The model with the lowest loss was saved as final model. Implementation was done using Pytorch. This architecture has previously been used and validated in (Wen et al., 2020). It is available through the ClinicaDL software available on GitHub: <https://github.com/aramis-lab/ClinicaDL>.

We compared this network to more sophisticated CNN architectures. In particular, we implemented a modified 3D version of Google’s incarnation of the Inception architecture (Szegedy et al., 2016). In addition we

also implemented a 3D ResNet (CNN with residual blocks) inspired from (Jónsson et al., 2019). More details about the architectures are given Figures S1 and S2. Both the Inception and the ResNet models were trained using the cross entropy loss weighted according to the proportion of images per class, the Adam optimizer with a learning rate of 1e-4 and the batch size was set to 2. These two models have been used in (Couvy-Duchesne et al., 2020) to predict brain age from 3D T1w MRI. For that specific task, they achieved a higher performance than the 5-layer CNN mentioned above. Their implementation is openly available on GitHub <https://github.com/aramis-lab/pac2019> and all the parameters of the CNNs are listed in the supplementary materials of (Couvy-Duchesne et al., 2020).

#### *2.4.2. Experiments*

Before starting the experiments, we defined a test set by randomly selecting 500 images which respected the same distribution of tiers as the images in the training/validation set. We also verified that the distribution of the manufacturers and the different scanner models was respected. The remaining 5000 images were split into training and validation using a 5-fold cross validation (CV). The separation between training, validation and test sets was made at the patient level to avoid data leakage. For each of the four tasks considered (SR, gadolinium, tier 3 vs 2-1, tier 2 vs 1), the five models trained in the CV were evaluated on the test set. We also studied the influence of the size of the training set on the performance by computing learning

Characteristics	Weighted Cohen’s kappa
SR (yes vs no)	0.88
Gadolinium injection (yes vs no)	0.89
Contrast (0 vs 1 vs 2)	0.79
Motion (0 vs 1 vs 2)	0.68
Noise (0 vs 1 vs 2)	0.70

Table 3: Weighted Cohen’s kappa between the two annotators

curves. We compared the output of each classifier with the consensus label. To set the automatic QC results in perspective, we computed the balanced accuracy (BA) for the raters (defined as the average of the BAs between each rater and the consensus).

### 3. Results

#### 3.1. Manual quality control

The inter-rater agreement was evaluated using the weighted Cohen’s kappa (Watson and Petrie, 2010) between the two annotators for each of the characteristics. Results are presented in Table 3. The agreement is strong for the SR label and the gadolinium injection (0.88 and 0.89) and moderate for the other characteristics (from 0.68 to 0.79).

The distribution of the consensus labels for the 5500 patients is shown in Figure 4. 26% of the images are labeled as SR, 16% as tier 1, 28% as tier 2, and 30% as tier 3. Table S1 reports the exact number of images for each

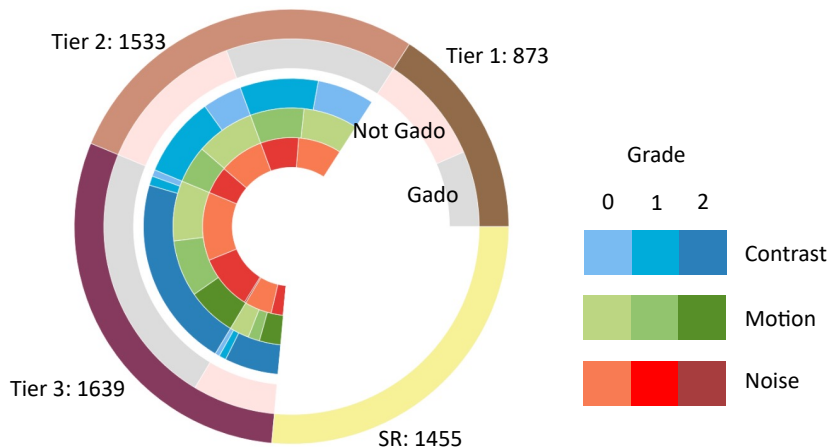


Figure 4: Distribution of the consensus labels for the whole dataset of 5500 images. Outer-most circle: images in SR and in the different tiers. For every tier, we divide between images with and without gadolinium injection. For each injection status we see the grade distribution of the contrast, motion and noise characteristics. This is also presented as a table (Table S1) in supplementary material so that the reader can have access to the exact numbers.

category. Figure 2 shows some representative examples of T1w brain images with the corresponding labels.

As expected, the proportion of images with gadolinium increased when the quality decreased (proportion of images with gadolinium: 41% in Tier 1, 53% in tier 2, 76% in tier 3;  $p < 2.13e^{-8}$ ;  $\chi^2$  test). A vast majority of tier 3 images had a contrast of 2 (90%) and were with gadolinium (70%).

If we analyse the relationships between characteristics, we note that 73% of images with a grade 2 for motion have also a grade 2 for contrast. Unsurprisingly, a strong motion has a severe impact on contrast. On the other hand, images with a grade 2 for contrast present a closer distribution of grade 0, 1 and 2 for motion (40%, 34%, and 26%, respectively).

	<b>Manufacturer</b> (%Siemens, %GE, % Philips, % Toshiba)	<b>Field strength</b> (%1.5T, %3T)	<b>Age</b> (mean $\pm$ std [range])	<b>Sex</b> (%F, %M)
<b>(Tier 1</b> <b>(n=702)</b>	90%, 10%, 0%, 0%**	9%, 91% **	47.51 $\pm$ 16.27 [18 - 88]	52%, 48%
<b>Tier 2</b> <b>(n=117)</b>	78%, 22%, 0.2%, 0.01%**	44%, 56%	54.42 $\pm$ 17.79 [18 - 95]	59%, 41%
<b>Tier 3</b> <b>(n=1323)</b>	38%, 62%, 0%, 0.2%**	60%, 40% **	59.97 $\pm$ 17.13 [18 - 85]	57%, 43%
<b>SR</b> <b>(n=1132)</b>	67%, 32%, 1%, 0%	28%, 72% **	54.95 $\pm$ 18.01 [18 - 93]	47%, 53%
<b>Total</b> <b>(n=4274)</b>	65%, 35%, 0.2%, 0%	39%, 61%	55.15 $\pm$ 17.89 [18 - 95]	53%, 46%

Table 4: Distribution of the manufacturers, field strength, sex and age according to QC grading (performed by the human raters) and on the overall population. We report the percentage of each manufacturer, field strength and sex, and the mean  $\pm$  standard deviation with the range for age. The analysis was restricted to the sub-population for which demographic information was available (4274 of 5500 images). Results with \*\* mean that the distributions between the overall population and a specific QC class were statistically significantly different (corrected  $p < 0.05$ ).

We studied the influence of the age, sex, manufacturer and field strength for the SR images or the different tiers for which demographic information was available (4274 out of 5500). In Table 4, we report the percentage of each manufacturer, field strength and sex, and the mean, standard deviation and range for the age according to the QC grading performed by the human raters (SR, tier 1, tier 2 or tier 3). We compared the distribution of the four overall quality classes to the overall population using a  $\chi^2$  test for the manufacturer, field strength and sex, and with a t-test for the age. P-values were corrected for multiple comparisons using Bonferroni correction. We

found statistically significant differences (corrected p-value  $<0.05$ ) for the manufacturer for tier 1, tier 2 and tier 3 and for the field strength for tier 1, tier 3 and SR. Specifically, in tier 1 and tier 2, there was a majority of Siemens machines (especially of 3T for tier 1), while in tier 3 there was a majority of GE Healthcare machines. In addition, the SR category contained many 3T images that are actually segmented images, as such processed images are usually available with the most recent machines (that come equipped with segmentation software). For age and sex, there was no significant difference.

DICOM attributes often contain information regarding the injection of gadolinium. However, it is well-known to radiologists that such information is often unreliable because it is manually entered by the MRI radiographer. We aimed to assess the extent to which such information was unreliable. We thus analysed the “study description” and “series description” DICOM attributes of the images to check if the presence of gadolinium injection was noted. We considered that it was noted if at least one of the words ‘gado’, ‘inj’ or ‘iv’ was present in the value of one of the attributes. Among the 2416 images that were manually annotated as with gadolinium, 2033 images had the information in the DICOM attributes. Among the 1629 images that were manually annotated as without gadolinium, 987 were noted as images with gadolinium injection according to the DICOM attributes. Since our manual annotation of gadolinium injection is highly reproducible and was designed with the guidance of an experienced neuroradiologist, we conclude that, as expected, DICOM attributes do not provide reliable information regarding

<b>Metric</b>	<b>SR (yes vs no)</b>	<b>Gadolinium injection (yes vs no)</b>	<b>Tier 3 vs tiers 2-1</b>	<b>Tier 2 vs tier 1</b>
BA annotators	97.13	96.10	91.56	88.27
BA classifiers	93.76 $\pm$ 0.57	97.14 $\pm$ 0.34	83.51 $\pm$ 0.93	71.65 $\pm$ 2.15
F1 score	94.85 $\pm$ 0.41	97.04 $\pm$ 0.31	84.07 $\pm$ 1.02	74.10 $\pm$ 1.35
MCC	85.71 $\pm$ 1.11	94.00 $\pm$ 0.64	67.38 $\pm$ 2.13	42.10 $\pm$ 3.25
AUC	93.76 $\pm$ 0.57	97.14 $\pm$ 0.34	83.51 $\pm$ 0.93	71.65 $\pm$ 2.15
Sensitivity	91.83 $\pm$ 1.18	96.45 $\pm$ 0.34	79.88 $\pm$ 3.06	77.39 $\pm$ 4.29
Specificity	95.69 $\pm$ 0.53	97.82 $\pm$ 0.62	87.14 $\pm$ 3.14	65.92 $\pm$ 7.47
PPV	86.44 $\pm$ 1.43	98.33 $\pm$ 0.46	81.93 $\pm$ 3.36	83.20 $\pm$ 2.31
NPV	97.51 $\pm$ 0.35	95.39 $\pm$ 0.42	85.83 $\pm$ 1.49	57.78 $\pm$ 2.63

Table 5: Results of the CNN classifier for all the tasks. We report the BA of the annotators and for every metric of the CNN we report the mean and the empirical standard deviation across the five folds. BA: balanced accuracy; MCC: Matthews correlation coefficient; AUC: area under the receiver operator characteristic curve; PPV: positive predictive values; NPV: negative predictive values

the presence of gadolinium. This highlights the importance of being able to detect it using an automatic QC tool.

### 3.2. Automatic quality control

Results obtained for the four tasks of interest by the proposed Conv5\_FC3 classifier are presented in Table 5. We report the BA of the annotators for comparison. For the recognition of SR images, we used all the images available in the training/validation set ( $n = 5000$ ); for the gadolinium and tier 3 vs tiers 2-1 tasks, the training/validation set does not include SR images ( $n = 3770$ ); and for the tier 2 vs tier 1 task, the training/validation set does not include SR and tier 3 images ( $n = 2182$ ).

Balanced accuracy for SR and gadolinium is excellent (94% and 97%). For SR, the CNN is slightly less good than the annotators. For gadolinium,

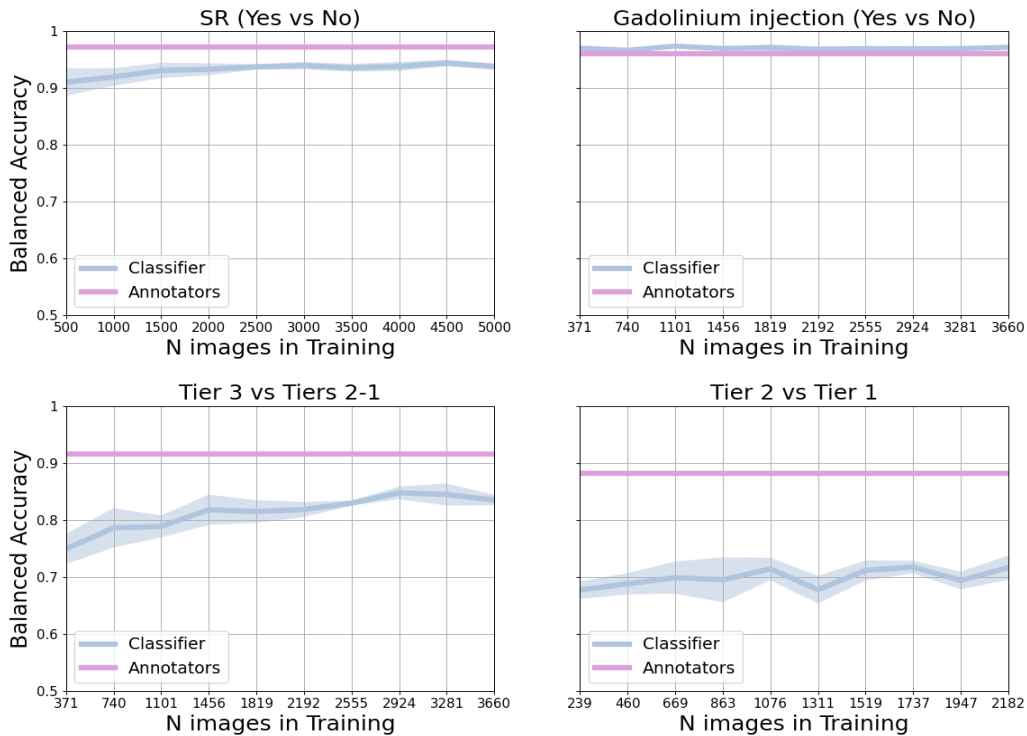


Figure 5: Learning curves for the SR (yes vs no), gadolinium injection (yes vs no), tier 3 vs tier 2-1 and tier 2 vs tier 1 tasks. Blue: balanced accuracy of the classifier across the five folds. Violet: balanced accuracy of the annotators on the testing set.

the CNN is as good as the raters. For tier 3 vs 2-1, the classifier BA is good but lower than that of the annotators. For tier 2 vs 1, CNN BA is low (71%) and much lower than that of the raters (88%).

The influence of the size of the training set on the performance is shown in Figure 5. For SR, the performance increases with sample size, even if it is also good with few examples (90% for 500 images) because of the easiness of the task. For gadolinium, performance is very high regardless of the sample size. For tier 3 vs tiers 2-1, adding more training samples helps the classifier

while this is not the case for tier 2 vs 1.

For tier 3 vs tiers 2-1 and tier 2 vs tier 1, we compared the proposed architecture, Conv5\_FC3, with the Inception and ResNet architectures. For both tasks, the balanced accuracy obtained with the different networks is comparable: while for tier 3 vs tiers 2-1 it is slightly higher with the ResNet ( $85.82 \pm 0.95$ ) than the Conv5\_FC3 ( $83.51 \pm 0.93$ ) and the Inception ( $82.40 \pm 1.2$ ), for tier 2 vs 1 it is slightly higher with the Conv5\_FC3 ( $71.65 \pm 2.15$ ) than the ResNet ( $68.08 \pm 1.6$ ) or Inception ( $69.27 \pm 2.05$ ) architectures. For both tasks, the performance of the different classifiers were not statistically different (for tier 3 vs tiers 2-1:  $p > 0.21$ , McNemar’s test; for tier 2 vs tier 1:  $p > 0.12$ , McNemar’s test). All the metrics are reported in Table 6. For the images in the test set having information about age and sex (372 out of 500 images) we studied the influence of age, sex, manufacturer and field strength of the scanner on the classification performance of all the models of our work. Specifically, we tested for differences in balanced accuracy using the Mann-Whitney U rank test and p-values were corrected for multiple comparisons using Bonferroni correction. No factor had a statistically significant influence on the classification performance (all corrected p-values  $> 0.05$ ).

### A. Tier 3 vs tiers 2-1

Metric	Conv5_FC3	Inception	ResNet
BA	83.51 ± 0.93	82.41 ± 1.28	85.82 ± 0.95
Sensitivity	79.88 ± 3.06	75.53 ± 2.68	80.75 ± 3.24
Specificity	87.14 ± 3.14	89.29 ± 3.45	90.89 ± 2.22
F1 score	84.07 ± 1.02	83.38 ± 1.44	86.57 ± 0.81
MCC	67.38 ± 2.13	66.08 ± 3.02	72.52 ± 1.70
AUC	83.51 ± 0.93	82.41 ± 1.28	85.82 ± 2.81
PPV	81.93 ± 3.36	83.80 ± 3.93	86.58 ± 2.43
NPV	85.83 ± 1.49	83.58 ± 1.20	86.85 ± 1.76

### B. Tier 2 vs tier 1

Metric	Conv5_FC3	Inception	ResNet
BA	71.65 ± 2.15	69.28 ± 2.81	68.08 ± 1.63
Sensitivity	77.39 ± 4.29	76.86 ± 4.76	82.35 ± 2.90
Specificity	65.92 ± 7.47	61.69 ± 10.01	53.80 ± 4.99
F1 score	74.10 ± 1.35	72.28 ± 1.13	72.94 ± 1.18
MCC	42.10 ± 3.25	37.74 ± 4.10	37.13 ± 2.73
AUC	71.65 ± 2.15	69.28 ± 2.81	68.08 ± 1.62
PPV	83.20 ± 2.32	81.51 ± 3.08	79.40 ± 1.34
NPV	57.78 ± 2.63	55.49 ± 1.70	58.77 ± 2.40

Table 6: Results of three 3D CNN architectures (Conv5\_FC3, Inception and ResNet) for the rating of the overall image quality. We report the mean and the empirical standard deviation across the five folds for all the metrics. BA: balanced accuracy; MCC: Matthews correlation coefficient; AUC: area under the receiver operator characteristic curve; PPV: positive predictive values; NPV: negative predictive values

## 4. Discussion

In this work, we developed a method for the automatic QC of T1w brain MRI for a large clinical data warehouse. Our approach allows: i) discarding images which are of no interest (SR), ii) recognizing gadolinium injection , iii) rating the overall image quality. To this aim, different CNN were trained and evaluated thanks to the manual annotation of 5500 images by two raters.

In the last decades, many computer-aided diagnosis systems using machine learning methods have been proposed for the detection of lesions or tumours, or for the classification of neurodegenerative or psychiatric diseases (Rathore et al., 2017; Işın et al., 2016; Burgos et al., 2021). Algorithms were mainly developed and tested using research images (Samper-González et al., 2018; Noor et al., 2019; Cuingnet et al., 2011), or clinical datasets of limited size (Morin et al., 2020; Zhang et al., 2019; Campese et al., 2019; Oh et al., 2019). Their validation on large realistic clinical datasets is crucial. To that aim, clinical data warehouses, which may gather millions of clinical routine images, offer fantastic opportunities. They also provide considerable challenges. In particular, selecting adequate images for a given analysis task can be very difficult: DICOM attributes may be unreliable, images may be of the wrong type, truncated and their quality is extremely variable. Therefore, automatic curation and QC methods are needed to fully exploit the potential of clinical data warehouses. Important efforts and achievements have been made by the scientific community to propose protocols and automatic tools for QC. MRIQC (Esteban et al., 2017) and VisualQC (Raamana

et al., 2020) are two tools developed for the QC of T1w brain MRI data: they propose the extraction of image quality metrics for the detection of outliers, and a graphical interface to check the images. Alfaro-Almagro et al. (2018) proposed a pipeline for the UK Biobank dataset. Sujit et al. (2019) trained a CNN using the research dataset ABIDE. Other works focused on QC of processing results (segmentation) rather than raw data (Keshavan et al., 2018; Klapwijk et al., 2019). However, all these tools were designed for research data. Even if the data came from multiple sites, they do not cover all the images existing in a clinical PACS: they did not cover images with gadolinium and the patients presented with a limited number of diseases. Indeed, research datasets do not contain SR or tier 3 images and they may have very few tier 2 images. Protocols for the acquisition of research data are often different (in particular, scanning time is often longer) and a systematic visual QC is often performed. If the quality of an image is poor, a second scan can be acquired and information about the image quality is provided. In addition, DICOM fields are standardized among a research dataset, meaning that from the modality name it is possible to recognise whether a gadolinium-based contrast agent has been injected or not. On the contrary, in a clinical data warehouse, we may find images with or without gadolinium injection, “research quality” images, and images segmented, cropped or with so much motion that it is impossible to distinguish the brain. This heterogeneity makes it impossible to use other QC tools present in the literature. In particular, software tools such as MRIQC Esteban et al. (2017) propose

an extensive image pre-processing pipeline before the calculation of image quality metrics. Classical neuroimaging software tools, such as SPM, ANTS or FSL, are typically validated only on T1w brain MRI of a good quality and without gadolinium. The quality of our data, in particular of SR images that represent 25% of our dataset and the fact that we have about 44% of images with gadolinium injection, does not allow us to trust the metrics extracted from segmentations. To the best of our knowledge, we are the first to propose an automatic QC framework for clinical data warehouses.

To train our automatic QC algorithm, we had to manually annotate a large sample of images from the data warehouse. It was not possible to use existing protocols and software tools. In addition to the limitations mentioned above, we were also constrained by the environment of the data warehouse which only included a Jupyter notebook and a command-line interface. While constraints may vary from a data warehouse to another, it is very common that the data cannot be downloaded and thus have to be used within a specific informatics set-up (Daniel and Salamanca, 2020). We thus developed a dedicated visual QC protocol, with the assistance of a resident radiologist. We compared the annotation using 3D images and 2D slices, and we concluded that three 2D slices were sufficient and could represent a good compromise to fulfil our objectives: one being the exclusion of bad quality images that would compromise further analyses. Manual annotation results showed that our protocol is reproducible across all tasks, even though agreement was weaker for more challenging characteristics. Inter-rater agreement

was strong for the SR label and the gadolinium injection and moderate for other characteristics. Manual annotation also provides interesting information on the variability of image quality in a clinical routine data warehouse. As much as 25% are totally unusable (SR), and almost a third has a very low quality (Tier 3). We also confirmed that gadolinium has a strong impact on image quality, hence the critical importance of detecting it accurately, the DICOM attributes being unreliable in that regard.

For detecting straight reject, our CNN had excellent performance (BA greater than 90%). Even though the task is relatively easy, this is very important in order to automatically discard images in a very large scale study. This was also the case for detection of gadolinium, an important characteristic that strongly impacts the behavior of many image analysis methods. For the rating of image quality, the situation was different for identifying Tier 3 (low quality) images and for separating Tier 2 (medium quality) and Tier 1 (high quality). The proposed CNN classifier identified low quality images (Tier 3) with a high accuracy (83%). This is important because these are typically the images on which image processing algorithms could fail. Differentiating images of high and medium quality could also be useful but is less important as both categories can likely lead to reliable diagnostic predictions. We thus believe that these tools can be reliably used on the rest of this large data warehouse and already have an important practical impact. We compared several more sophisticated CNN architectures to our simple network based on five convolutional and three fully connected layers. How-

ever, these more complex networks (3D Inception and 3D ResNet) did not provide any significant improvement in performance. We could not compare our approach with the more standard ones based on the extraction of the image quality metrics since the software tools are not adapted to our data: we can trust the results of a classifier based on these types of features only if we trust the segmentation results. Our aim was to propose a framework for the QC that can be re-used on a clinical platform and so must be adapted to different tasks and have a preprocessing as light as possible. This is the reason why we developed a CNN for all the tasks.

Thanks to the large number of hospitals in the AP-HP consortium (39 hospitals) and to the huge amount of images collected over the years (1980–now), we strongly believe that this dataset is representative of 3D T1w brain MRI that may be acquired in other hospitals. Consequently, the use of our QC framework could be generalized and it represents a first important step for the use of clinical data warehouses for the design of computer-aided diagnosis systems. Indeed, this work on quality control can help researchers to conduct studies, from observational studies that include MRI-based measurements to the development of CAD systems. First, obviously, the system will help save time by excluding SR images since they are not usable at all, both for training and testing. Even a neuroradiologist would not rely on these images for diagnostic purposes. Thereafter, the graded quality is also useful: either by controlling this confounding factor that can impact classification results or results of correlative studies, or by excluding images of bad quality (i.e.

tier 3) when training the CAD. The quality grade could also contribute to building a confidence score for a classifier: when performing inference on a bad quality image we could lower the confidence in the classifier's result. Our study is going to be useful when performing research studies of different kinds (from training machine learning models to observational clinical retrospective studies). It is true that, beyond research, it could potentially be useful in a clinical routine setting. However, several steps would be needed towards that aim. First, it would obviously need to be approved as a medical device (e.g. FDA or CE approval). The most natural way to integrate it would probably be within the software provided by the MRI vendor. The computer hardware associated with the MRI machine is certainly powerful enough to perform the inference steps of our models. In a clinical routine setting, there are several potential usages of the approach. The most natural may be to associate it to automatic quantification algorithms which are more and more commonly available within the radiologist console. This would help flag exams for which, due to image quality, quantification cannot be considered reliable.

The main limitations of our study concern the annotation process. With the analysis of only three slices, we limit the chances to notice localised artefacts. Another consequence is that it may be difficult to properly distinguish the characteristics when an image is degraded: in particular the motion and the noise may be confused. This is also reflected by moderate values of the weighted Cohen's kappa obtained for these two characteristics. Additionally,

even if we believe that the CNN models that were trained on data from the AP-HP data warehouse can be applied to other clinical datasets due to the large numbers of hospitals and scanner models involved in study and to the extended period of time, it would be beneficial to apply them on a public dataset for benchmarking. Furthermore, it would be interesting to study the potential association between the diagnoses of the patients and the quality of the images and the performance of the automatic QC. However, such a study is not straightforward to conduct due to the multiplicity of diagnostic codes for a given inpatient and the absence of any diagnostic information for outpatients. This is left for future work.

## 5. Conclusion

In this work, we proposed a framework for the automatic quality control of 3D brain T1w MRI for a large clinical data warehouse. Thanks to the manual annotation of 5500 images, we trained and validated different convolutional neural networks on 5000 images with a 5-fold CV and we tested them on an independent test set of 500 images. The classifier was as efficient as manual rating for the classification of images which are not proper 3D T1w brain MRI (i.e. truncated or segmented images) and for the images for which gadolinium was injected. In addition, the classifier was able to recognise low quality images with good accuracy.

## **Acknowledgments**

The research was done using the Clinical Data Warehouse of the Greater Paris University Hospitals. The authors are grateful to the members of the AP-HP WIND and URC teams, and in particular Stéphane Bréant, Florence Tubach, Jacques Ropers, Antoine Rozès, Camille Nevoret, Christel Daniel, Martin Hilka, Yannick Jacob, Julien Dubiel and Cyrina Saussol. They would also like to thank the “Collégiale de Radiologie of AP-HP” as well as, more generally, all the radiology departments from AP-HP hospitals. Finally, the authors are very appreciative of the support and guidance they have received from Quentin Vanderbecq when setting up the visual quality control protocol.

The research leading to these results has received funding from the Abeona Foundation (project Brain@Scale), from the French government under management of Agence Nationale de la Recherche as part of the “Investissements d’avenir” program, reference ANR-19-P3IA-0001 (PRAIRIE 3IA Institute) and reference ANR-10-IAIHU-06 (Agence Nationale de la Recherche-10-IA Institut Hospitalo-Universitaire-6).

## **Authors contribution**

Study concepts and study design: OC, NB, DD, SB

Acquisition, analysis or interpretation of data: all authors

Manuscript drafting or manuscript revision for important intellectual content: all authors

Approval of final version of submitted manuscript: all authors

Literature research: SB, NB, OC

Statistical analysis: SB

Obtained funding: OC, NB

Administrative, technical, or material support: AM

Study supervision: OC, NB, DD

## **Disclosure statement**

Competing financial interests related to the present article: none to disclose for all authors.

Competing financial interests unrelated to the present article: OC reports

having received consulting fees from AskBio (2020), having received fees for writing a lay audience short paper from Expression Santé (2019). Members from his laboratory have co-supervised a PhD thesis with myBrainTechnologies (2016-2019) and with Qynapse (2017-present). OC's spouse is an employee and holds stock-options of myBrainTechnologies (2015-present). O.C. holds a patent registered at the International Bureau of the World Intellectual Property Organization (PCT/IB2016/0526993, Schiratti J-B, Allasonniere S, Colliot O, Durrleman S, A method for determining the temporal progression of a biological phenomenon and associated methods and devices) (2017).

### **APPRIMAGE Study Group**

Olivier Colliot, Ninon Burgos, Simona Bottani <sup>1</sup>  
Didier Dormont <sup>1,2</sup>, Samia Si Smail Belkacem, Sebastian Ströer <sup>2</sup>  
Nathalie Boddaert <sup>3</sup>  
Farida Benoudiba, Ghaida Nasser, Claire Ancelet, Laurent Spelle <sup>4</sup>  
Hubert Ducou-Le-Pointe<sup>5</sup>  
Catherine Adamsbaum<sup>6</sup>  
Marianne Alison<sup>7</sup>  
Emmanuel Houdart<sup>8</sup>  
Robert Carlier <sup>9,17</sup>  
Myriam Edjlali<sup>9</sup>  
Betty Marro<sup>10,11</sup>  
Lionel Arrive<sup>10</sup>  
Alain Luciani<sup>12</sup>  
Antoine Khalil<sup>13</sup>  
Elisabeth Dion<sup>14</sup>  
Laurence Rocher<sup>15</sup>  
Pierre-Yves Brillet<sup>16</sup>  
Paul Legmann, Jean-Luc Drape <sup>18</sup>  
Aurélien Maire, Stéphane Bréant, Christel Daniel, Martin Hilka, Yannick Jacob, Julien Dubiel, Cyrina Saussol <sup>19</sup>  
Florence Tubach, Jacques Ropers, Antoine Rozès, Camille Nevoret <sup>20</sup>

<sup>1</sup> Paris Brain Institute (ICM), Inserm U 1127, CNRS UMR 7225, Sorbonne Université, Inria, Aramis project-team, F-75013, Paris, France

<sup>2</sup> AP-HP, Hôpital de la Pitié Salpêtrière, Department of Neuroradiology, F-75013, Paris, France

- <sup>3</sup> AP-HP, Hôpital Necker, Department of Radiology, F-75015, Paris, France
- <sup>4</sup> AP-HP, Hôpital Bicêtre, Department of Radiology, F-94270, Le Kremlin-Bicêtre, France
- <sup>5</sup> AP-HP, Hôpital Armand-Trousseau, Department of Radiology, F-75012, Paris, France
- <sup>6</sup> AP-HP, Hôpital Bicêtre, Department of Pediatric Radiology, F-94270, Le Kremlin-Bicêtre, France
- <sup>7</sup> AP-HP, Hôpital Robert-Debré, Department of Radiology, F-75019, Paris, France
- <sup>8</sup> AP-HP, Hôpital Lariboisière, Department of Neuroradiology, F-75010, Paris, France
- <sup>9</sup> AP-HP, Hôpital Raymond-Poincaré, Department of Radiology, F-92380, Garches, France
- <sup>10</sup> AP-HP, Hôpital Saint-Antoine, Department of Radiology, F-75012, Paris, France
- <sup>11</sup> AP-HP, Hôpital Tenon, Department of Radiology, F-75020, Paris, France
- <sup>12</sup> AP-HP, Hôpital Henri-Mondor, Department of Radiology, F-94000, Créteil, France
- <sup>13</sup> AP-HP, Hôpital Bichat, Department of Radiology, F-75018, Paris, France
- <sup>14</sup> AP-HP, Hôpital Hôtel-Dieu, Department of Radiology, F-75004, Paris, France
- <sup>15</sup> AP-HP, Hôpital Antoine-Béclère, Department of Radiology, F-92140, Clamart, France
- <sup>16</sup> AP-HP, Hôpital Avicenne, Department of Radiology, F-93000, Bobigny, France
- <sup>17</sup> AP-HP, Hôpital Ambroise Paré, Department of Radiology, F-92100 104, Boulogne-Billancourt, France
- <sup>18</sup> AP-HP, Hôpital Cochin, Department of Radiology, F-75014, Paris, France
- <sup>19</sup> AP-HP, WIND department, F-75012, Paris, France
- <sup>20</sup> AP-HP, Unité de Recherche Clinique, Hôpital de la Pitié Salpêtrière, Department of Neuroradiology, F-75013, Paris, France

## References

- Alba, X., Lekadir, K., Pereanez, M., Medrano-Gracia, P., Young, A.A., Frangi, A.F., 2018. Automatic initialization and quality control of large-scale cardiac mri segmentations. *Medical image analysis* 43, 129–141.
- Alfaro-Almagro, F., Jenkinson, M., Bangerter, N.K., Andersson, J.L.R., Griffanti, L., Douaud, G., Sotiropoulos, S.N., Jbabdi, S., Hernandez-Fernandez, M., Vallee, E., Vidaurre, D., Webster, M., McCarthy, P., Rorden, C., Daducci, A., Alexander, D.C., Zhang, H., Dragonu, I., Matthews, P.M., Miller, K.L., Smith, S.M., 2018. Image processing and Quality Control for the first 10,000 brain imaging datasets from UK Biobank. *Neuroimage* 166, 400–424.
- Amara, N., Lamouchi, O., Gattoufi, S., 2020. Design of a Breast Image Data Warehouse Framework, in: 2020 International Multi-Conference on: “Organization of Knowledge and Advanced Technologies” (OCTA), IEEE. pp. 1–13.
- Avants, B.B., Epstein, C.L., Grossman, M., Gee, J.C., 2008. Symmetric diffeomorphic image registration with cross-correlation: evaluating automated labeling of elderly and neurodegenerative brain. *Medical Image Analysis* 12, 26–41.
- Avants, B.B., Tustison, N.J., Stauffer, M., Song, G., Wu, B., Gee, J.C., 2014. The Insight ToolKit image registration framework. *Frontiers in Neuroinformatics* 8, 44.
- Burgos, N., Bottani, S., Faouzi, J., Thibeau-Sutre, E., Colliot, O., 2021. Deep learning for brain disorders: from data processing to disease treatment. *Briefings in Bioinformatics* 22, 1560–1576.
- Burgos, N., Colliot, O., 2020. Machine learning for classification and prediction of brain diseases: recent advances and upcoming challenges. *Current Opinion in Neurology* 33, 439–450.
- Campanella, G., Rajanna, A.R., Corsale, L., Schüffler, P.J., Yagi, Y., Fuchs, T.J., 2018. Towards machine learned quality control: A benchmark for sharpness quantification in digital pathology. *Computerized Medical Imaging and Graphics* 65, 142–151.

- Campese, S., Lauriola, I., Scarpazza, C., Sartori, G., Aioli, F., 2019. Psychiatric disorders classification with 3D convolutional neural networks, in: INNS Big Data and Deep Learning Conference, Springer. pp. 48–57.
- Choi, H., Ha, S., Kang, H., Lee, H., Lee, D.S., 2019. Deep learning only by normal brain PET identify unheralded brain anomalies. *EBioMedicine* 43, 447–453.
- Couvy-Duchesne, B., Faouzi, J., Martin, B., Thibeau-Sutre, E., Wild, A., Ansart, M., Durrleman, S., Dormont, D., Burgos, N., Colliot, O., 2020. Ensemble Learning of Convolutional Neural Network, Support Vector Machine, and Best Linear Unbiased Predictor for Brain Age Prediction: ARAMIS Contribution to the Predictive Analytics Competition 2019 Challenge. *Frontiers in Psychiatry* 11.
- Cuingnet, R., Gerardin, E., Tessieras, J., Auzias, G., Lehéricy, S., Habert, M.O., Chupin, M., Benali, H., Colliot, O., 2011. Automatic classification of patients with Alzheimer’s disease from structural MRI: a comparison of ten methods using the ADNI database. *NeuroImage* 56, 766–781.
- Daniel, C., Salamanca, E., 2020. Hospital Databases, in: *Healthcare and Artificial Intelligence*. Springer, pp. 57–67.
- Di Martino, A., Yan, C.G., Li, Q., Denio, E., Castellanos, F.X., Alaerts, K., Anderson, J.S., Assaf, M., Bookheimer, S.Y., Dapretto, M., Deen, B., Delmonte, S., Dinstein, I., Ertl-Wagner, B., Fair, D.A., Gallagher, L., Kennedy, D.P., Keown, C.L., Keyzers, C., Lainhart, J.E., Lord, C., Luna, B., Menon, V., Minshew, N.J., Monk, C.S., Mueller, S., Müller, R.A., Nebel, M.B., Nigg, J.T., O’Hearn, K., Pelphrey, K.A., Peltier, S.J., Rudie, J.D., Sunaert, S., Thioux, M., Tyszka, J.M., Uddin, L.Q., Verhoeven, J.S., Wenderoth, N., Wiggins, J.L., Mostofsky, S.H., Milham, M.P., 2014. The autism brain imaging data exchange: towards a large-scale evaluation of the intrinsic brain architecture in autism. *Molecular Psychiatry* 19, 659–667.
- Dong, J., Liu, S., Liao, Y., Wen, H., Lei, B., Li, S., Wang, T., 2019. A generic quality control framework for fetal ultrasound cardiac four-chamber planes. *IEEE journal of biomedical and health informatics* 24, 931–942.

- Esteban, O., Birman, D., Schaer, M., Koyejo, O.O., Poldrack, R.A., Gorgolewski, K.J., 2017. MRIQC: Advancing the automatic prediction of image quality in MRI from unseen sites. *PLOS One* 12, e0184661.
- Falahati, F., Westman, E., Simmons, A., 2014. Multivariate data analysis and machine learning in Alzheimer’s disease with a focus on structural magnetic resonance imaging. *Journal of Alzheimer’s disease* 41, 685–708.
- Frisoni, G.B., Fox, N.C., Jack, C.R., Scheltens, P., Thompson, P.M., 2010. The clinical use of structural MRI in Alzheimer disease. *Nature Reviews Neurology* 6, 67–77. doi:10.1038/nrneuro1.2009.215.
- Gilmore, A., Buser, N., Hanson, J.L., 2019. Variations in structural MRI quality impact measures of brain anatomy: Relations with age and other sociodemographic variables. *Biorxiv* , 581876.
- Gorgolewski, K.J., Auer, T., Calhoun, V.D., Craddock, R.C., Das, S., Duff, E.P., Flandin, G., Ghosh, S.S., Glatard, T., Halchenko, Y.O., Handwerker, D.A., Hanke, M., Keator, D., Li, X., Michael, Z., Maumet, C., Nichols, B.N., Nichols, T.E., Pellman, J., Poline, J.B., Rokem, A., Schaefer, G., Sochat, V., Triplett, W., Turner, J.A., Varoquaux, G., Poldrack, R.A., 2016. The brain imaging data structure, a format for organizing and describing outputs of neuroimaging experiments. *Scientific data* 3, 1–9.
- Graham, M.S., Drobnjak, I., Zhang, H., 2018. A supervised learning approach for diffusion mri quality control with minimal training data. *NeuroImage* 178, 668–676.
- Harper, L., Fumagalli, G.G., Barkhof, F., Scheltens, P., O’Brien, J.T., Bowman, F., Burton, E.J., Rohrer, J.D., Fox, N.C., Ridgway, G.R., Schott, J.M., 2016. MRI visual rating scales in the diagnosis of dementia: evaluation in 184 post-mortem confirmed cases. *Brain* 139, 1211–1225.
- Işın, A., Direkoğlu, C., Şah, M., 2016. Review of MRI-based brain tumor image segmentation using deep learning methods. *Procedia Computer Science* 102, 317–324.
- Jack, C.R., Bernstein, M.A., Fox, N.C., Thompson, P., Alexander, G., Harvey, D., Borowski, B., Britson, P.J., L. Whitwell, J., Ward, C., Dale, A.M., Felmlee, J.P., Gunter, J.L., Hill, D.L., Killiany, R., Schuff, N., Fox-Bosetti, S., Lin, C., Studholme, C., DeCarli, C.S., Gunnar Krueger, Ward,

- H.A., Metzger, G.J., Scott, K.T., Mallozzi, R., Blezek, D., Levy, J., Deb-  
bins, J.P., Fleisher, A.S., Albert, M., Green, R., Bartzokis, G., Glover,  
G., Mugler, J., Weiner, M.W., ADNI Study, 2008. The Alzheimer’s dis-  
ease neuroimaging initiative (ADNI): MRI methods. *Journal of Magnetic  
Resonance Imaging* 27, 685–691.
- Janowczyk, A., Zuo, R., Gilmore, H., Feldman, M., Madabhushi, A., 2019.  
Histoqc: an open-source quality control tool for digital pathology slides.  
*JCO clinical cancer informatics* 3, 1–7.
- Jónsson, B.A., Bjornsdottir, G., Thorgeirsson, T., Ellingsen, L.M., Walters,  
G.B., Gudbjartsson, D., Stefansson, H., Stefansson, K., Ulfarsson, M.,  
2019. Brain age prediction using deep learning uncovers associated se-  
quence variants. *Nature Communications* 10, 1–10.
- Keshavan, A., Datta, E., McDonough, I.M., Madan, C.R., Jordan, K., Henry,  
R.G., 2018. Mindcontrol: A web application for brain segmentation quality  
control. *NeuroImage* 170, 365–372.
- Kim, H., Irimia, A., Hobel, S.M., Pogosyan, M., Tang, H., Petrosyan, P.,  
Blanco, R.E.C., Duffy, B.A., Zhao, L., Crawford, K.L., Liew, S.L., Clark,  
K., Law, M., Mukherjee, P., Manley, G.T., Van Horn, J.D., Toga, A.W.,  
2019. LONI QC system: a semi-automated, web-based and freely-available  
environment for the comprehensive quality control of neuroimaging data.  
*Frontiers in Neuroinformatics* 13, 60.
- Klapwijk, E.T., Van De Kamp, F., Van Der Meulen, M., Peters, S., Wierenga,  
L.M., 2019. Qoala-T: A supervised-learning tool for quality control of  
FreeSurfer segmented MRI data. *NeuroImage* 189, 116–129.
- Koikkalainen, J., Rhodius-Meester, H., Tolonen, A., Barkhof, F., Tijms, B.,  
Lemstra, A.W., Tong, T., Guerrero, R., Schuh, A., Ledig, C., Rueckert,  
D., Soininen, H., Remes, A.M., Waldemar, G., Hasselbalch, S., Mecocci,  
P., van der Flier, W., Lötjönen, J., 2016. Differential diagnosis of neurode-  
generative diseases using structural MRI data. *NeuroImage: Clinical* 11,  
435–449.
- Kretz, T., Müller, K.R., Schaeffter, T., Elster, C., 2020. Mammography im-  
age quality assurance using deep learning. *IEEE Transactions on Biomed-  
ical Engineering* 67, 3317–3326.

- Küstner, T., Gatidis, S., Liebgott, A., Schwartz, M., Mauch, L., Martirosian, P., Schmidt, H., Schwenzer, N.F., Nikolaou, K., Bamberg, F., et al., 2018. A machine-learning framework for automatic reference-free quality assessment in mri. *Magnetic resonance imaging* 53, 134–147.
- Li, X., Morgan, P.S., Ashburner, J., Smith, J., Rorden, C., 2016. The first step for neuroimaging data analysis: DICOM to NIfTI conversion. *Journal of Neuroscience Methods* 264, 47–56.
- Littlejohns, T.J., Holliday, J., Gibson, L.M., Garratt, S., Oesingmann, N., Alfaro-Almagro, F., Bell, J.D., Boultonwood, C., Collins, R., Conroy, M.C., Crabtree, N., Doherty, N., Frangi, A.F., Harvey, N.C., Leeson, P., Miller, K.L., Neubauer, S., Petersen, S.E., Sellors, J., Sheard, S., Smith, S.M., Sudlow, C.L.M., Matthews, P.M., Allen, N.E., 2020. The UK Biobank imaging enhancement of 100,000 participants: rationale, data collection, management and future directions. *Nature Communications* 11, 1–12.
- Morin, A., Samper-Gonzalez, J., Bertrand, A., Ströer, S., Dormont, D., Mendes, A., Coupé, P., Ahdidan, J., Lévy, M., Samri, D., Hampel, H., Dubois, B., Teichmann, M., Epelbaum, S., Colliot, O., 2020. Accuracy of MRI Classification Algorithms in a Tertiary Memory Center Clinical Routine Cohort. *Journal of Alzheimer’s Disease* 74, 1157–1166.
- Noor, M.B.T., Zenia, N.Z., Kaiser, M.S., Mahmud, M., Al Mamun, S., 2019. Detecting neurodegenerative disease from MRI: A brief review on a deep learning perspective, in: *International Conference on Brain Informatics*, Springer. pp. 115–125.
- Oh, K., Kim, W., Shen, G., Piao, Y., Kang, N.I., Oh, I.S., Chung, Y.C., 2019. Classification of schizophrenia and normal controls using 3D convolutional neural network and outcome visualization. *Schizophrenia Research* 212, 186–195.
- Oksuz, I., Ruijsink, B., Puyol-Antón, E., Clough, J.R., Cruz, G., Bustin, A., Prieto, C., Botnar, R., Rueckert, D., Schnabel, J.A., et al., 2019. Automatic cnn-based detection of cardiac mr motion artefacts using k-space data augmentation and curriculum learning. *Medical image analysis* 55, 136–147.

- Punjabi, A., Martersteck, A., Wang, Y., Parrish, T.B., Katsaggelos, A.K., 2019. Neuroimaging modality fusion in Alzheimer’s classification using convolutional neural networks. *PloS one* 14, e0225759.
- Raamana, P.R., Theyers, A., Selliah, T., Bhati, P., Arnott, S.R., Hassel, S., Scott, C.J.M., Harris, J., Zamyadi, M., Lam, R.W., Milev, R., Mueller, D.J., Rotzinger, S., Frey, B.N., Kennedy, S.H., Black, S.E., Lang, A., Masellis, M., Symons, S., Bartha, R., MacQueen, G.M., CAN-BIND Investigator Team, ONDRI Study Group, Strother, S.C., 2020. Visual QC Protocol for FreeSurfer Cortical Parcellations from Anatomical MRI. *bioRxiv* .
- Rathore, S., Habes, M., Iftikhar, M.A., Shacklett, A., Davatzikos, C., 2017. A review on neuroimaging-based classification studies and associated feature extraction methods for Alzheimer’s disease and its prodromal stages. *NeuroImage* 155, 530–548.
- Reuter, M., Tisdall, M.D., Qureshi, A., Buckner, R.L., van der Kouwe, A.J., Fischl, B., 2015. Head motion during MRI acquisition reduces gray matter volume and thickness estimates. *NeuroImage* 107, 107–115.
- Robinson, R., Oktay, O., Bai, W., Valindria, V.V., Sanghvi, M.M., Aung, N., Paiva, J.M., Zemrak, F., Fung, K., Lukaschuk, E., et al., 2018. Real-time prediction of segmentation quality, in: *International Conference on Medical Image Computing and Computer-Assisted Intervention*, Springer. pp. 578–585.
- Robinson, R., Valindria, V.V., Bai, W., Oktay, O., Kainz, B., Suzuki, H., Sanghvi, M.M., Aung, N., Paiva, J.M., Zemrak, F., et al., 2019. Automated quality control in image segmentation: application to the uk biobank cardiovascular magnetic resonance imaging study. *Journal of Cardiovascular Magnetic Resonance* 21, 1–14.
- Routier, A., Burgos, N., Díaz, M., Bacci, M., Bottani, S., El-Rifai, O., Fontanella, S., Gori, P., Guillon, J., Guyot, A., Hassanaly, R., Jacquemont, T., Lu, P., Marcoux, A., Moreau, T., Samper-González, J., Teichmann, M., Thibeau–Sutre, E., Vaillant, G., Wen, J., Wild, A., Habert, M.O., Durrleman, S., Colliot, O., 2021. Clinica: An Open Source Software Platform for Reproducible Clinical Neuroscience Studies. hal-02308126 URL: <https://hal.inria.fr/hal-02308126>.

- Sadri, A.R., Janowczyk, A., Zhou, R., Verma, R., Beig, N., Antunes, J., Madabhushi, A., Tiwari, P., Viswanath, S.E., 2020. Mrqy—an open-source tool for quality control of mr imaging data. *Medical Physics* 47, 6029–6038.
- Samper-González, J., Burgos, N., Bottani, S., Fontanella, S., Lu, P., Marcoux, A., Routier, A., Guillon, J., Bacci, M., Wen, J., Bertrand, A., Bertin, H., Habert, M.O., Durrleman, S., Evgeniou, T., Colliot, O., 2018. Reproducible evaluation of classification methods in Alzheimer’s disease: Framework and application to MRI and PET data. *NeuroImage* 183, 504–521.
- Sujit, S.J., Coronado, I., Kamali, A., Narayana, P.A., Gabr, R.E., 2019. Automated image quality evaluation of structural brain MRI using an ensemble of deep learning networks. *Journal of Magnetic Resonance Imaging* 50, 1260–1267.
- Sunoqrot, M.R., Selnæs, K.M., Sandsmark, E., Nketiah, G.A., Zavala-Romero, O., Stoyanova, R., Bathen, T.F., Elschot, M., 2020. A quality control system for automated prostate segmentation on t2-weighted mri. *Diagnostics* 10, 714.
- Szegedy, C., Vanhoucke, V., Ioffe, S., Shlens, J., Wojna, Z., 2016. Rethinking the inception architecture for computer vision, in: *Proceedings of the IEEE Conference on Computer Vision and Pattern Recognition*, pp. 2818–2826.
- Tayari, N., Obels, J., Kobus, T., Scheenen, T.W., Heerschap, A., 2019. Simple and broadly applicable automatic quality control for 3d 1h mr spectroscopic imaging data of the prostate. *Magnetic resonance in medicine* 81, 2887–2895.
- Tustison, N.J., Avants, B.B., Cook, P.A., Zheng, Y., Egan, A., Yushkevich, P.A., Gee, J.C., 2010. N4ITK: improved N3 bias correction. *IEEE Transactions on Medical Imaging* 29, 1310–1320.
- Watson, P., Petrie, A., 2010. Method agreement analysis: a review of correct methodology. *Theriogenology* 73, 1167–1179.
- Wen, J., Thibeau-Sutre, E., Diaz-Melo, M., Samper-González, J., Routier, A., Bottani, S., Dormont, D., Durrleman, S., Burgos, N., Colliot, O., 2020. Convolutional Neural Networks for Classification of Alzheimer’s Disease: Overview and Reproducible Evaluation. *Medical Image Analysis* , 101694.

Zhang, J., Li, X., Li, Y., Wang, M., Huang, B., Yao, S., Shen, L., 2019. Three dimensional convolutional neural network-based classification of conduct disorder with structural MRI. *Brain Imaging and Behavior* , 1–8.

# Automatic quality control of brain T1-weighted magnetic resonance images for a clinical data warehouse

Simona Bottani<sup>a,b,c,d,e,f</sup>, Ninon Burgos<sup>b,c,d,e,f,a</sup>, Aurélien Maire<sup>g</sup>, Adam Wild<sup>b,c,d,e,f,a</sup>, Sebastian Ströer<sup>h</sup>, Didier Dormont<sup>b,c,d,e,f,a,h</sup>, Olivier Colliot<sup>b,c,d,e,f,a</sup>, APPRIMAGE Study Group

<sup>a</sup>Inria, Aramis project-team, Paris, 75013, France

<sup>b</sup>Sorbonne Université, Paris, 75013, France

<sup>c</sup>Institut du Cerveau - Paris Brain Institute - ICM, Paris, 75013, France

<sup>d</sup>Inserm, Paris, 75013, France

<sup>e</sup>CNRS, Paris, 75013, France

<sup>f</sup>AP-HP, Hôpital de la Pitié Salpêtrière, Paris, 75013, France

<sup>g</sup>AP-HP, WIND department, Paris, 75012, France

<sup>h</sup>AP-HP, Hôpital de la Pitié Salpêtrière, Department of Neuroradiology, Paris, 75013, France

-

## Supplementary Material

<b>QC grading</b>	<b>N</b>	<b>Gadolinium injection</b>	<b>N</b>	<b>Contrast Grade</b>	<b>N</b>	<b>Motion Grade</b>	<b>N</b>	<b>Noise Grade</b>	<b>N</b>
Tier 1	873	With gado	358	-	-	-	-	-	-
		Without gado	515	-	-	-	-	-	-
Tier 2	1533	With gado	812	0	342	0	409	0	431
				1	470	1	403	1	381
		Without gado	721	0	237	0	441	0	445
				1	484	1	280	1	276
Tier 3	1639	With gado	1246	0	40	0	451	0	683
				1	56	1	425	1	549
				2	1150	2	370	2	14
		Without gado	393	0	27	0	147	0	271
				1	43	1	86	1	120
				2	323	2	160	2	2
SR	1455	-	-	-	-	-	-	-	-

Table S1: For each QC grading, we report the total number of images, the number of images with or without gadolinium injection and the number of images per grade for the contrast, motion and noise characteristics.

Layer	Filter size	Number of filters/ neurons	Stride size	Padding size	Dropout rate	Output size
Conv+BN+ReLU - 1	3x3x3	8	1	1	-	8x169x208x179
MaxPool - 1	2x2x2	-	2	adaptive	-	8x85x104x90
Conv+BN+ReLU - 2	3x3x3	16	1	1	-	16x85x104x90
MaxPool - 2	2x2x2	-	2	adaptive	-	16x43x52x45
Conv+BN+ReLU - 3	3x3x3	32	1	1	-	32x43x52x45
MaxPool - 3	2x2x2	-	2	adaptive	-	32x22x26x23
Conv+BN+ReLU - 4	3x3x3	64	1	1	-	64x22x26x23
MaxPool - 4	2x2x2	-	2	adaptive	-	64x11x13x1
Conv+BN+ReLU - 5	3x3x3	128	1	1	-	128x11x13x12
MaxPool - 5	2x2x2	-	2	adaptive	-	128x6x7x6
Dropout	-	-	-	-	0.5	128x6x7x6
FC - 1	-	1300	-	-	-	1500
FC - 2	-	50	-	-	-	50
FC - 3	-	2	-	-	-	2
Softmax	-	-	-	-	-	2

Table S2: Hyperparameters of the 3D Conv5\_FC3 CNN. BN: batch normalization; Conv: convolutional layer; FC: fully connected; MaxPool: max pooling.

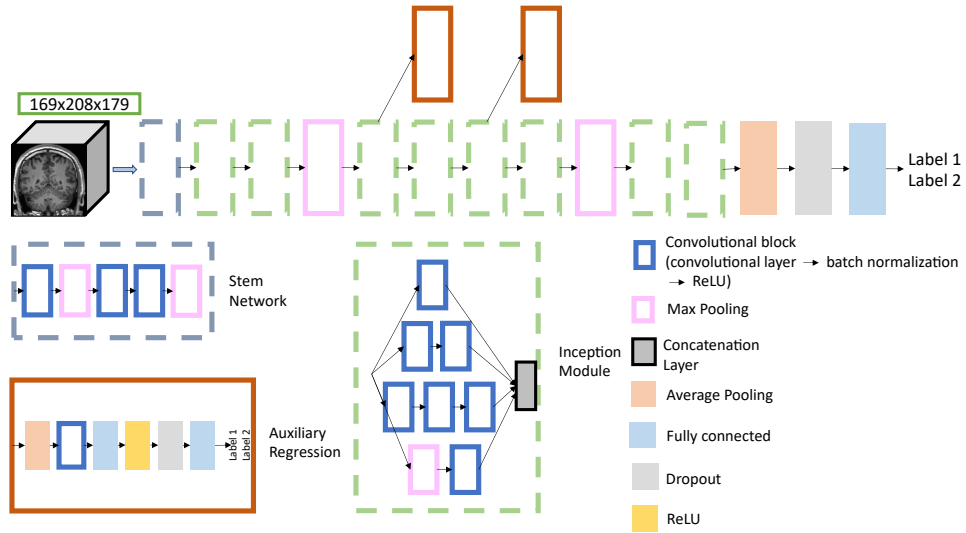


Figure S1: Architecture of the Inception 3D CNN. More information regarding the hyper-parameters can be found in (Couvry-Duchesne et al., 2020).

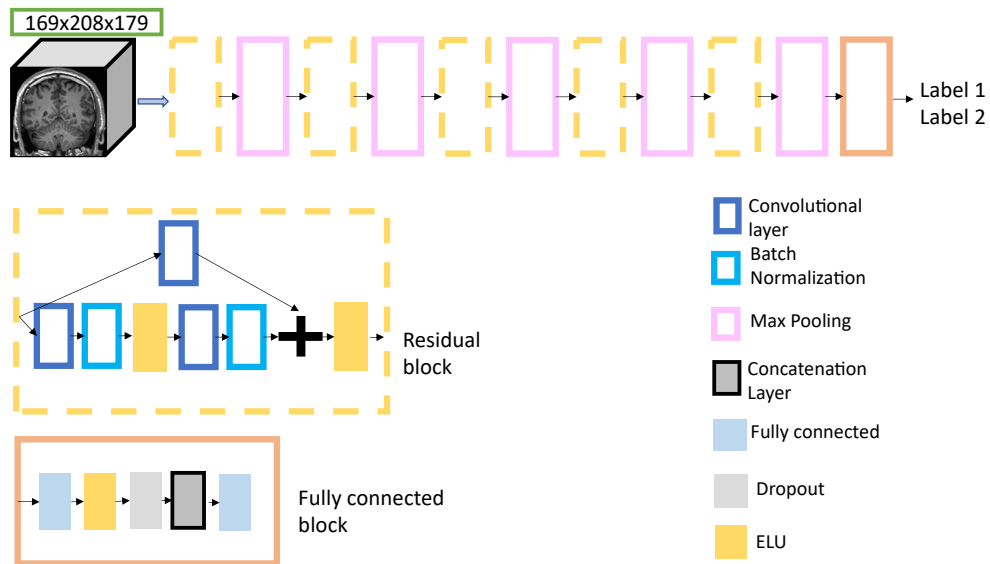


Figure S2: Architecture of the ResNet 3D CNN. More information regarding the hyper-parameters can be found in (Couvry-Duchesne et al., 2020).